SOME OBSERVATIONS OF HYPERVELOCITY IMPACTS WITH POROUS MEDIA

By Donald E. Gault, Ezra D. Heitowit, and Henry J. Moore (Geol. Survey)

NASA. Space Sciences Division
Ames Research Center,
Moffett Field, California

ABSTRACT

High-speed framing camera records are presented for Pyrex glass spheres impacting with porous targets at velocities from 5.8 to 7.1 km/sec. Target porosities varied from approximately 43 percent for particulate materials to 70 percent for a pumice and 87 percent for a macroscale model of the Hapke fairy castle structure. In all cases, fragmented material was ejected from the craters formed by the impact. Mass-size distributions of the ejecta fragments are presented for several of the experiments.

Author

INTRODUCTION

The fragmentation and ejection of material from the lunar surface resulting from the impact of interplanetary bodies and particles has been analyzed recently (Gault, Shoemaker, and Moore, 1963) on the basis of experimental studies of hypervelocity impact in rock and sand. The analysis shows that the flux of fragments of a given

[1] U. S. Geological Survey, Menlo Park, California

Presented at the Conf. on Lunar Surface Materials, Boston, 21-23 May 1963

mass which are ejected from the lunar surface can be expected to be at least three and probably four orders of magnitude greater than the flux of the impacting bodies and particles of the same mass which produce the ejected fragmental material. Most of the fragments will be ejected from the lunar surface with velocities less than the lunar escape velocity. These fragments must ultimately fall back on the lunar surface and cause "secondary" impact events.

The tremendous increase in the number of impacts on the lunar surface caused by the secondary events is significant both to plans for manned and unmanned exploration of the Moon and to the interpretation of the evolutionary processes which have brought the Moon to its present state. Gault, et al. (ref. 1) suggest that a cloud of fragments is continually flying across the lunar surface; that is, with the continuous flux of interplanetary debris impacting the lunar surface, the steady and repeated production of secondary fragments will result in the formation of a "steady-state" cloud of ejected material following ballistic trajectories across the lunar surface. Such a cloud, which has been estimated to have a spatial density at the lunar surface of from 10^5 to 10^7 times that for the interplanetary bodies and particles, would pose a hostile environment for lunar probes and vehicles. Fortunately, the hazard of catastrophic punctures in vehicles from secondary impacts is low, perhaps almost nil, because of the relatively low energies of most of the individual fragments.

It is of more immediate significance to the Lunar Surface Materials Conference, however, that the results of the impact studies support a model for the lunar surface which is composed of a mixed rubble of unsorted rock fragments ranging in size from large blocks to submicron-sized particles. Moreover, in view of the higher flux rates for the smallest particles of interplanetary debris and crater ejecta, it seems reasonable to infer that the surface rubble has been and is being continually abraded to finer sizes. Over geological time, therefore, small voids and cracks may have gradually filled with pulverized rock and, in addition, a mantle of fine particles may have spread over the entire lunar surface.

Whether or not the individual grains in a dust-like mantle will assume an orientation similar to the fairy castle structure described by Hapke (1963) is problematical, but certainly the abrasive action by interplanetary debris and secondary particles is a mechanism for providing the basic ingredients for a porous or dendroidal material on the lunar surface. One important question immediately arises, therefore, in regard to the validity of the analytical results and interpretations based on the study of impact in a solid rock (basalt). For a preliminary answer to this question, Gault, et al., present results for craters formed in a weakly bonded quartz sand (35- to 40-percent porosity) and conclude that the results derived from impact in solid rock for the flux of secondary fragments are conservative. However, McCracken and Dubin (1963) argue that extremely porous structures with porosities near 90 percent will effectively

swallow up an impacting particle and preclude the formation of secondary fragments. Such an inhibiting effect by a porous medium would greatly attenuate any cloud of fragments flying above the surface and, at the same time, reduce the erosion rate of rubble and the rate at which a mantle of fine material would build up on the lunar surface.

Clearly, the differences in the phenomenon of impact in solid and porous materials must be clarified before a realistic assessment can be made of the effects of impact on the lunar environment and surface. It is toward such a clarification that the present note has been prepared on the basis of the currently available results from studies of hypervelocity impact in porous media. The major fraction of the results presented herein are photographic records of the impacts of 1/8-inch (3.18 mm) diameter Pyrex glass spheres into targets composed of particulate (sand) material (43- to 47-percent porosity), a pumice (70-percent porosity), and a macroscale model of the fairy castle structure[2] (87-percent porosity). The impact velocities varied from 5.8 to 7.1 km/sec. Mass-size distributions of the fragments ejected during crater formation are presented for several of the target media.

[2]The authors are indebted to T. P. Meloy, Allis-Chalmers Manufacturing Company, Milwaukee, Wisconsin, for furnishing the macroscale model of the fairy castle structure for these tests.

PHOTOGRAPHIC RECORDS

Framing Camera Records

Selected frames from high-speed motion picture records of seven impact events in porous media are shown in figures 1 through 7. A summary of pertinent data on the experimental conditions for each impact are included in the accompanying table.

TABLE I.- SUMMARY OF EXPERIMENTAL CONDITIONS FOR PHOTOGRAPHIC RECORDS OF IMPACT EVENTS PRESENTED IN FIGURES 1-7

Round	Target material	Nominal grain size, mm	Bulk density, g/cc	Percent porosity	Impact angle, deg	Impact velocity, km/sec	Camera speed, frames/sec	Figure
SP663	Quartz, feldspar, and lithic sand (bonded)	3 (2.1 to 4.2)	1.4 ± 0.1	47	90 (normal)	5.8	1.06×10^{6}	1
SP732	Pumice	- - -	0.67 ± 0.05	71	90	6.5	1.09×10^{6}	2
SP733	Quartz sand (bonded)	0.5 (0.35 to 0.70)	1.5 ± 0.1	43	90	6.2	0.95×10^{6}	3
SP681	Quartz, feldspar, and lithic sand (bonded)	3 (2.1 to 4.2)	1.4 ± 0.1	47	90	6.1	7.1×10^{3}	4
SP680	Quartz, feldspar, and lithic sand (bonded)	3 (2.1 to 4.2)	1.4 ± 0.1	47	45	6.3	7.2×10^{3}	5
SP676	Quartz, feldspar, and lithic sand (unbonded)	3 (2.1 to 4.2)	1.4 ± 0.1	47	30	6.7	7.3×10^{3}	6
SP871	Quartz, chert (Fairy castle)	8 (5 to 10)	0.3 ± 0.1	87	90	7.1	7.5×10^{3}	7

Note: 1/8 inch (3.18 mm) diameter Pyrex glass spheres (mass = 0.037g) used as projectiles. All impacts occurred in a nitrogen atmosphere of approximately 75 mm Hg.

The first three figures present records obtained at a nominal framing rate of 10^6 frames/sec to illustrate the ejection of fragments during the earliest stages of impact in porous materials. The remaining figures, results for framing rates of 7 to 7.5×10^3 frames/sec, illustrate entire cratering sequences and show, in particular, the late stages of the cratering process during which most of the ejecta is thrown out of a crater. Figures 4, 5, and 6 demonstrate, moreover, the effects of oblique impact and, to some extent, the effect of target strength on the crater dimensions and mass of material excavated by the impacts.

These photographic records are significant in several respects, foremost of which is the graphic proof they provide that fragments can be ejected from a variety of porous targets including the macroscale fairy castle structure. The impacts shown in figures 1, 4, 5, 6, and 7 are especially notable since the grain sizes and pore spaces of the targets are equal to or, for the fairy castle, considerably greater than the dimensions of the projectile. Although the experimental conditions are different from those previously reported by Gault, et al. (1963) for basalt and 0.3-mm sand, the ejection of fragmental material would seem to be relatively unaffected. Further discussion of this point will be made later.

In addition to the salient observation that material was ejected from all the impact craters, five specific observations noted in the photographic records are worthy of mention here:

1. The phenomenon of jetting which contributes to the ejection of ultra high-speed material from the point of impact (Gault, et al., 1963; Gault and Heitowit, 1963) is inhibited, but not eliminated, with porous media. Although probably not discernible in the figure reproductions accompanying this paper, the original negatives and first generation prints of the records reveal that some jetting occurred with pumice and the 0.5-mm grain sand targets (figs. 2 and 3, respectively). The records are inadequate for evaluating ejection velocities associated with the jetting, but subsequent to the jetting process, ejection velocities between 2 and 5 km/sec are evident. Similar velocities occurred for the ejecta produced by impact in the 3-mm grain material (fig. 1). It appears, therefore, that even with a porous surface, impact on the moon will inject some material into cislunar and interplanetary space.

2. In contrast to the relatively symmetrical radial distribution of the ejecta first emanating from the embryonic craters formed in basalt and the 0.3-mm sand reported by Gault, et al. (1963), impact in particulate materials with grains the same size as the projectile results in an initial ejection process in which filaments of fragments are squirted upward in random directions (fig. 1). Moreover, the ejection of these initial fragments seems to be delayed for 5 or 6 microseconds after the projectile contacts the face of the target material. A preliminary explanation for these observations is that some initial compression and closure of the target pore spaces takes place immediately below the projectile. The subsequent

ejection is delayed by this compression, but eventually material filters upward through partially closed pores in a random pattern. During the later stages of the crater formation, however, symmetry is established when the major fraction of the fragments is ejected.

3. Impact at oblique angles produces spray patterns which, except for jetting, are essentially symmetrical about an axis normal to the face of the target. This has been observed consistently for all impact events in solid and porous media and is clearly evident in figures 4, 5, and 6. Such a result together with the observations noted in the preceding paragraph strongly suggests that, with the exception of the high-velocity component of the ejecta (most of which probably escapes the lunar gravitational field), material thrown out of impact craters should be symmetrically disposed around the point of impact regardless of the obliquity of the impact angle.

4. Comparison between figures 5 and 6 provides some insight into the effects of target strengths on the final dimensions of a crater. Although no measurements of the crater dimensions are possible for the unbonded material because of post-shot slumping (a result of tilting the target to angles just less than the angle of repose of the material), it appears that the craters formed in the bonded sand target (compressive strength approximately 10^7 to 10^8 dynes/cm^2) are two to three times smaller than craters in the unbonded targets. Whether or not a proportionate increase in ejected mass occurs for the unbonded material is subject to future

determination. The current results suggest that if the lunar surface is mantled with similar loose or weakly bonded particulate material, the estimates by Gault, et al., for the flux of secondary fragments are conservative when based on results of impacts in solid rock.

5. The photographic records taken at the lowest framing rate were recorded on color film and reveal in all cases that small intensely luminous bits of material are ejected from the craters. This material is presumed to be fused products of the impacts, an interpretation which is supported by the fact that fused material has been consistently identified during post-shot examination of the ejecta. For the particular case of the fairy castle impact, some of the incandescent spots were driven downward into the open pore spaces of the structure as well as up and outward in a manner similar to the events observed for the more dense media. For particles striking the lunar surface with full cosmic impact velocities, some vaporization of material should take place. Thus, it is tempting to speculate that the combination of vapor and melt driven into the substrata of such structures could provide a binding agent which, when combined with compaction resulting from multiple impacts, could produce a somewhat porous but cohesive material having some physical strength.

Target and Crater Records

Photographs of the resultant craters in the 3-mm grain, pumice, and 0.5-mm grain target materials are presented as figures 8, 9, and 10, respectively. The craters in the bonded sands are significantly larger and have a different shape than the crater in pumice.

The craters in the bonded particulate material are generally bowl shaped with poorly defined circumferential limits. Although not appropriate to the craters shown in the photographs, a lens of finely crushed rock flour has been observed to remain in the bottom of craters formed under similar conditions.

In marked contrast, the crater in the pumice is a bottle shaped cavity with a slightly larger subsurface diameter than the apparent diameter showing on the face of the target. The interior of the cavity and especially the bottom half is covered with fine flour and some fused material. The differences from the craters in particulate media are probably attributable to increased porosity, greater strength, and the cellular structure of the pumice.

The macroscale model of the fairy castle structure provided to the authors by T. P. Meloy is shown in figures 11 and 12 under two angles of illumination to illustrate its reflective properties. In figure 11, the light source is placed behind the camera, and in figure 12, the axis of the light source is displaced approximately 90° from the optical axis of the camera. The pronounced backscattering characteristics of the structure noted by Hapke (1963) is readily apparent.

The post-shot remains of the fairy castle target are shown in figures 13 and 14. The extent of the damage is somewhat surprising even when consideration is made for "edge" effects of the small target and the two large clusters of grains which appear to have been broken loose from the target and then tumbled from the target as a result of the gravitational forces at the completion of the event (fig. 13). A general view of the target in the ejecta-collector tank (fig. 14) shows the large number of individual grains which were disaggregated by the impact. No estimate can be made for the size of the "crater" produced in this structure.

EJECTA MASS-SIZE DISTRIBUTIONS

As in the previous studies of hypervelocity impact in rock reported by Gault, et al., ejecta from the craters formed in the porous targets have been collected to ascertain the mass-size distribution of the fragments. Reduction of these data is currently in progress and data are available for only three events. These results are presented as figures 15, 16, and 17 for, respectively, the ejecta produced by impact in a bonded 3-mm grain material similar to that shown in figures 1 and 4, the impact in pumice shown in figure 2, and the impact in 0.5-mm grain sand shown in figure 3. These size distributions are presented in logarithmic form as histograms of the fractional contribution from each size class and in terms of the cumulative mass of fragments finer than a given fragment size. It should be noted that the distribution shown in figure 15 has been

distorted in the fragment size classes equal to and larger than the nominal grain size of the target. The distortion was caused by the addition of considerable material which, inadvertently left unbonded during fabrication of the target, sloughed out of the target area after the cratering process was completed. Since this sloughed material would consist primarily of the nominal 3-mm grains and, perhaps, some clusters of grains, an estimated distribution for the event is shown that is consistent with the total mass ejected from other craters that did not slough under similar conditions, but for which size distributions are unavailable.

The size distributions for the ejecta from the bonded sand targets show similar trends. Most of the ejecta from the craters consist of disaggregated grains mixed with some partially disaggregated target material. It is only a small fraction of the ejected mass, the order of 10 percent, that evidences any fracturing or crushing of the original granular material. The slopes of the cumulative size distributions between 40 microns and the nominal grain size for the two targets are 0.5 and 0.35 for, respectively, the 3-mm and 0.5-mm sand. These values are remarkably similar to those previously reported by Gault, et al., for the fragments larger than 40 microns from craters in basalt (0.3 to 0.6). Moreover, the similarity in the cumulative distribution persists into the smaller fragment sizes. For fragments finer than approximately 40 microns, the slopes of the size distributions increase with decreasing fragment size and appear to be approaching a cut-off size for fragments with dimensions somewhat smaller than 0.1 micron.

The size distribution for the pumice ejecta, however, exhibits a trend which is unique in comparison to those for solid rock and particulate material. The latter have the bulk of the ejecta mass concentrated in the largest size classes, whereas most of the mass of pumice fragments is concentrated in the intermediate sizes between the largest and smallest fragment dimensions - between approximately 100 and 200 microns for the data shown in figure 16. The pumice cumulative curve, therefore, is no longer linear for the logarithmic presentation and instead yields a distribution in which the slope increases monotonically from a value of about 0.1 with decreasing fragment size. Data for the pumice fragments finer than 40 microns is unavailable at present, but presumably it will be similar, as indicated in figure 14, to the distributions for solid and particulate targets.

The total mass ejected from the particulate targets for the experimental impact velocities of approximately 6 km/sec is indicated in figures 15 and 17 to be 10^3 times the mass of the Pyrex projectiles. This value for the ejected mass, in agreement with the earlier results reported by Gault, et al., for aluminum impacts into a weakly bonded 0.3-mm sand, is approximately three times the mass thrown out of basalt craters.

In marked contrast, however, the mass ejected from the pumice crater is more than an order of magnitude smaller - only 40 times the mass of the Pyrex projectile (fig. 16). Clearly, impact in a

highly porous material with considerable physical strength, such as the pumice employed for this study, inhibits the formation of secondary fragments. Whether porosity or strength is the major factor controlling the total ejected mass remains to be determined, but it is worth noting here that, based on the photographic records, the increased porosity of the fairy castle structure does not appear to decrease the formation of secondary fragments. Moreover, when it is realized that the mass of each individual grain of the macroscale fairy castle structure is from four to eight times the mass of the Pyrex projectile, the photographic records, in lieu of more rigorous criteria, provide evidence that the total mass ejected from the "crater" in the fairy castle target exceeds the mass thrown out of the pumice target. This line of reasoning leads one to speculate that strength is the most important parameter controlling the ejection of material from craters formed in porous media. The difference in crater dimensions noted before between the bonded and unbonded 3-mm grain targets supports such a speculation.

CONCLUDING REMARKS

The experimental results presented demonstrate that the ejection of appreciable mass of fragmented debris from an impact crater is not unique to solid or low-porosity target materials. The results of the impact into the macroscale model of the fairy castle structure are believed to be of particular significance since fragments were ejected under conditions for which the projectile was small

with respect to the grain and pore size of the structure. Thus, by inference, the impact of microparticles of interplanetary debris can be effective in ejecting material from a similar porous material on the lunar surface into ballistic trajectories across the surface of the Moon. On the other hand, the effectiveness of the impacting interplanetary debris may be inhibited to some extent if the surface consists of a strong vesicular material similar to pumice. It is apparent that the experimental results obtained to date for the impact of Pyrex spheres into various porous targets constitutes strong, although not incontrovertible, evidence in support of the hypothesis of a "steady-state" cloud of fragments flying across the lunar surface.

REFERENCES

1. Gault, Donald E., Shoemaker, Eugene M., and Moore, Henry J.: Spray Ejected From the Lunar Surface by Meteoroid Impact. NASA TN D-1767, 1963.

2. Hapke, Bruce, and Van Horn, Hugh: Photometric Studies of Complex Surfaces, With Applications to the Moon. Journal Geophysical Res., vol. 68, no. 15, Aug. 1963, pp. 4545-4570.

3. McCracken, Curtis W., and Dubin, Maurice: Dust Bonbardment on the Lunar Surface. Lunar Surface Materials Conference, Boston, Mass., May 21-23, 1963.

4. Gault, Donald E., and Heitowit, Ezra D.: The Partition of Energy for Hypervelocity Impact Craters Formed in Rock. Proc. of the 6th Hypervelocity Impact Symposium, Cleveland, Ohio, April 30, May 1-2, 1963.

FIGURE TITLES

Figure 1.- Selected frames from a high-speed photographic record of a 1/8 inch (3.18 mm) diameter Pyrex sphere impacting a bonded particulate target composed of nominal 3-mm quartz grains; impact velocity, 5.8 km/sec; framing rate, 1.06×10^6 per second; 90° (normal) impact angle; numerical values indicate time in microseconds after impact.

Figure 2.- Selected frames from a high-speed photographic record of a 1/8 inch (3.18 mm) diameter Pyrex sphere impacting a pumice target; impact velocity, 6.5 km/sec; framing rate, 1.09×10^6 per second; 90° (normal) impact angle; numerical values indicate time in microseconds after impact.

Figure 3.- Selected frames from a high-speed photographic record of a 1/8 inch (3.18 mm) diameter Pyrex sphere impacting a bonded particulate target composed of nominal 0.8-mm quartz grains; impact velocity, 6.2 km/sec; framing rate, 0.95×10^6 per second; 90° (normal) impact angle; numerical values indicate time in microseconds after impact.

Figure 4.- Selected frames from a high-speed photographic record of a 1/8 inch (3.18 mm) diameter Pyrex sphere impacting a bonded particulate target composed of nominal 3-mm quartz grains; impact velocity, 6.1 km/sec; framing rate, 7.1×10^3 per second; 90° (normal) impact angle; numerical values indicate time in milliseconds after impact.

Figure 5.- Selected frames from a high-speed photographic record of a 1/8 inch (3.18 mm) diameter Pyrex sphere impacting a bonded particulate target composed of nominal 3-mm quartz grains; impact velocity, 6.3 km/sec; framing rate, 7.2×10^3 per second; 45° impact angle; numerical values indicate time in milliseconds after impact.

Figure 6.- Selected frames from a high-speed photographic record of a 1/8 inch (3.18 mm) diameter Pyrex sphere impacting an unbonded particulate target composed of nominal 3-mm quartz grains; impact velocity, 6.7 km/sec; framing rate, 7.3×10^3 per second; 30° angle of impact; numerical values indicate time in milliseconds after impact.

Figure 7.- Selected frames from a high-speed photographic record of a 1/8 inch (3.18 mm) diameter Pyrex sphere impacting a macroscale model of the fairy castle structure composed of nominal 8-mm quartz grains; impact velocity, 7.1 km/sec; framing rate, 7.5×10^3 per second; 90° (normal) impact angle; numerical values indicate time in milliseconds after impact.

Figure 8.- Crater formed in the 3 mm (nominal) grain target by the impact of a 1/8 inch (3.18 mm) diameter Pyrex sphere similar to the one displayed on the target; impact velocity, 5.8 km/sec.

Figure 9.- The crater formed in the pumice target by the impact of a 1/8 inch (3.18 mm) diameter Pyrex sphere similar to the one displayed on the target; impact velocity, 6.5 km/sec.

Figure 10.- The crater formed in the 0.5 mm (nominal) grain target by the impact of a 1/8 inch (3.18 mm) diameter Pyrex sphere similar to the one displayed on the target; impact velocity, 6.2 km/sec.

Figure 11.- Photograph of the macroscale model of the fairy castle structure with the illumination directly behind the camera.

Figure 12.- Photograph of the macroscale model of the fairy castle structure with the axis of the light source displaced 90° from the optical axis of the camera.

Figure 13.- Post-shot view of the macroscale model of the fairy castle structure after the impact of a 1/8 inch (3.18 mm) diameter Pyrex sphere; impact velocity, 7.1 km/sec.

Figure 14.- Post-shot view of the macroscale model of the fairy castle structure in the ejecta-collector tank.

Figure 15.- Mass-size distributions for the ejecta produced by the impact with the 3-mm (nominal) grain target.

Figure 16.- Mass-size distributions for the ejecta produced by the impact with the pumice target.

Figure 17.- Mass-size distributions for the ejecta produced by the impact in the 0.5-mm (nominal) grain target.

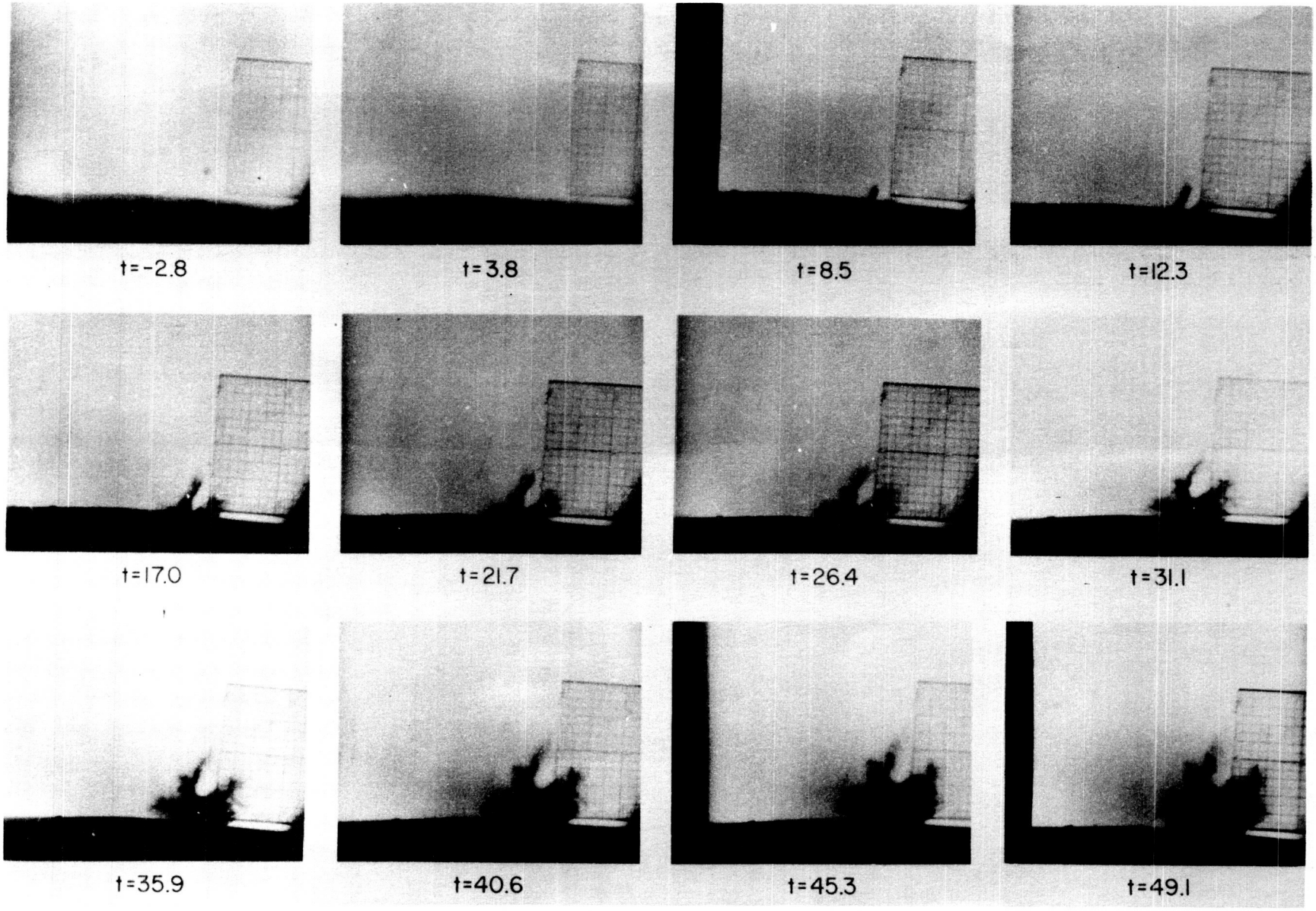

Figure 1.

A-31711

NATIONAL AERONAUTICS AND SPACE ADMINISTRATION
AMES RESEARCH CENTER, MOFFETT FIELD, CALIFORNIA

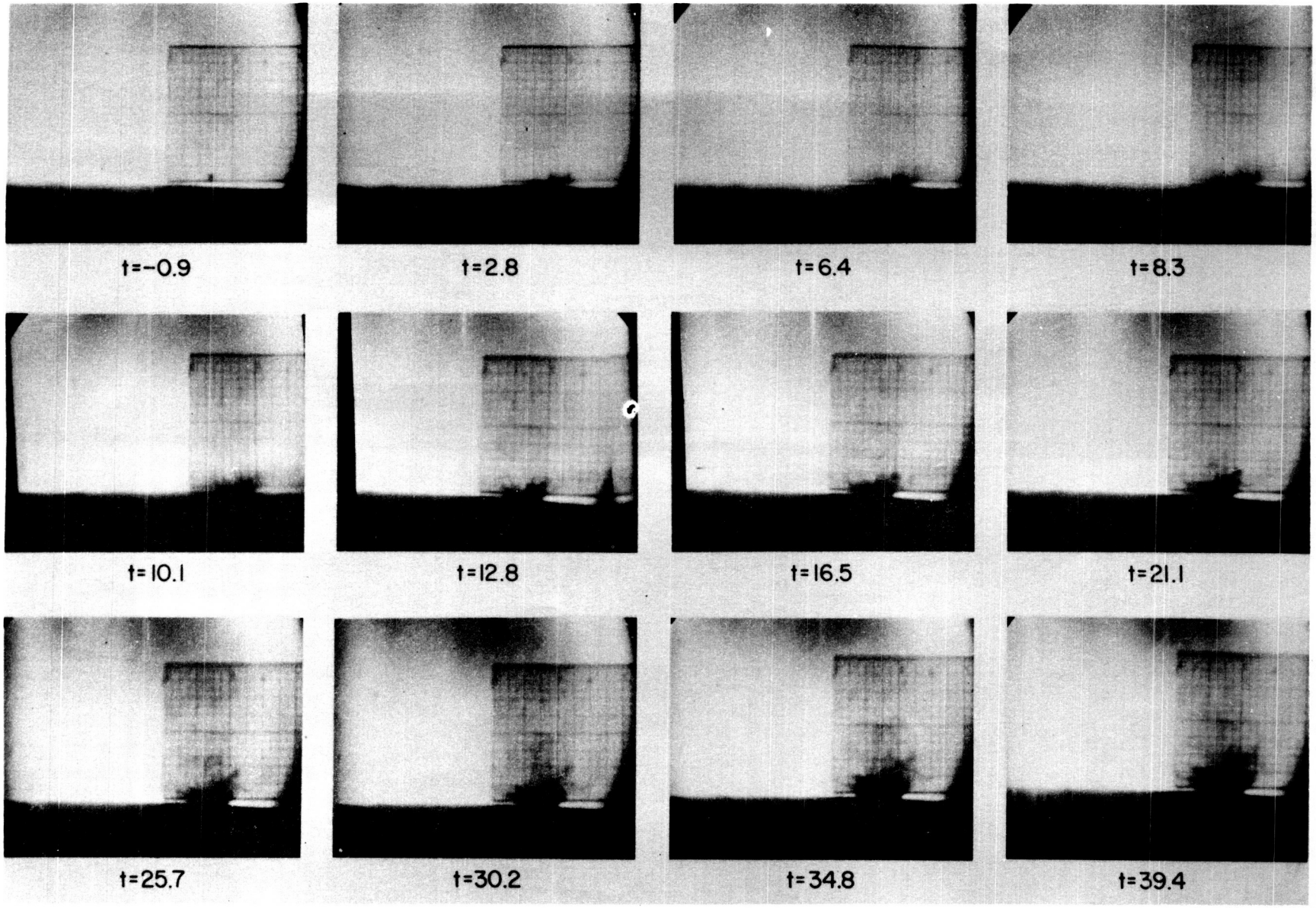

Figure 2.

A-31713

NATIONAL AERONAUTICS AND SPACE ADMINISTRATION
AMES RESEARCH CENTER, MOFFETT FIELD, CALIFORNIA

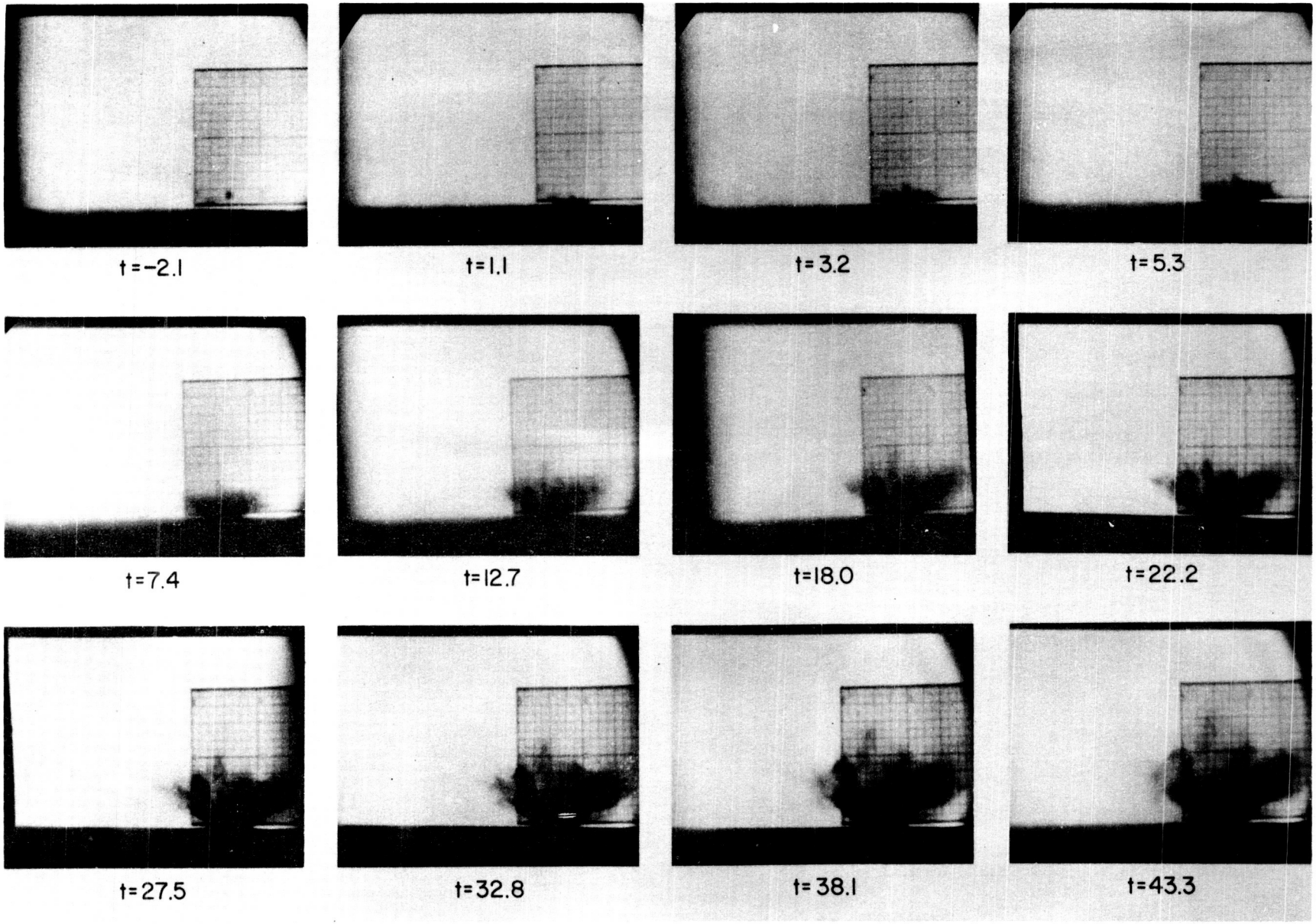

Figure 3.

A-31712

NATIONAL AERONAUTICS AND SPACE ADMINISTRATION
AMES RESEARCH CENTER, MOFFETT FIELD, CALIFORNIA

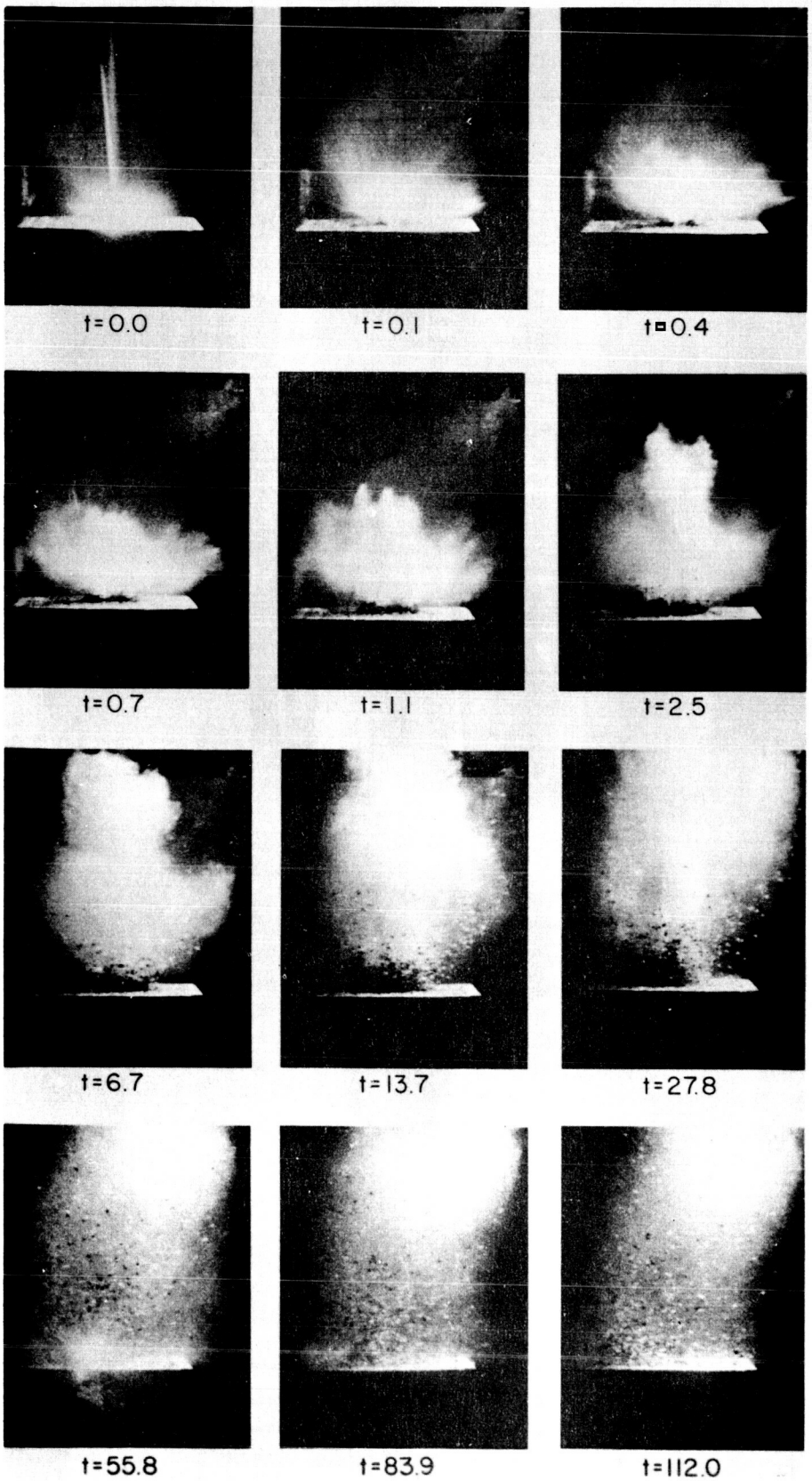

Figure 4.

A-31707

NATIONAL AERONAUTICS AND SPACE ADMINISTRATION
AMES RESEARCH CENTER, MOFFETT FIELD, CALIFORNIA

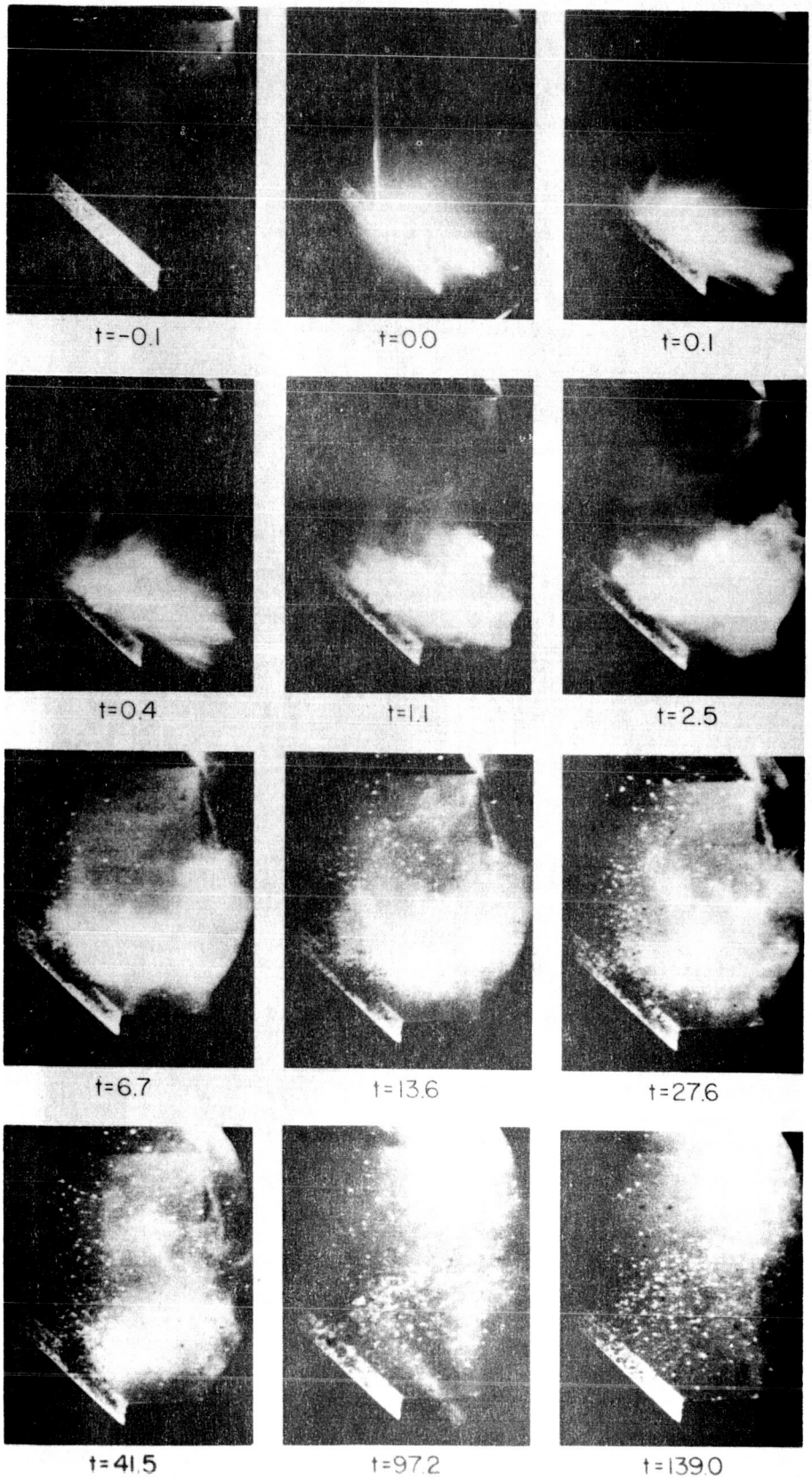

Figure 5.

A-31708

NATIONAL AERONAUTICS AND SPACE ADMINISTRATION
AMES RESEARCH CENTER, MOFFETT FIELD, CALIFORNIA

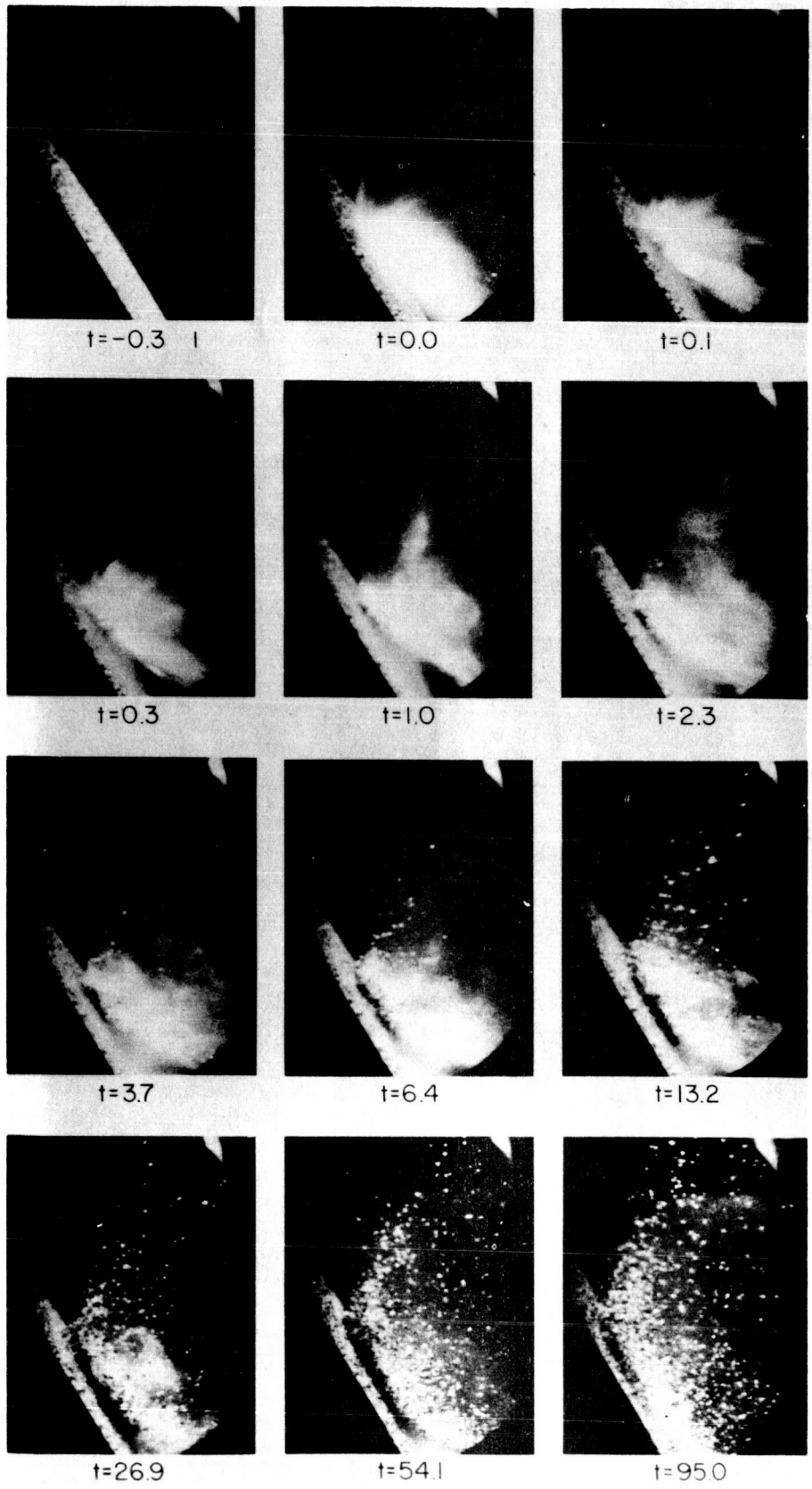

Figure 6.

A-31709

NATIONAL AERONAUTICS AND SPACE ADMINISTRATION
AMES RESEARCH CENTER, MOFFETT FIELD, CALIFORNIA

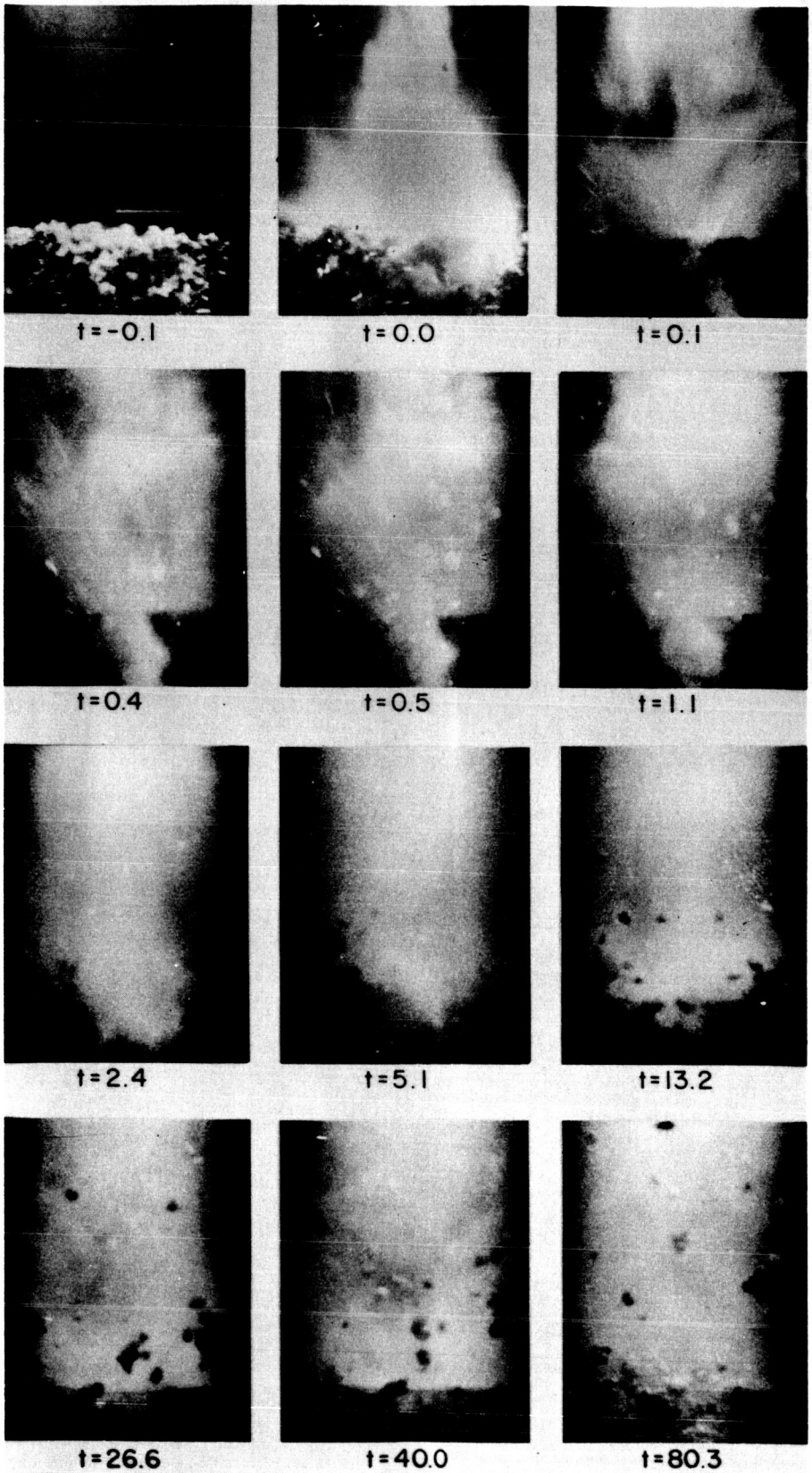

Figure 7.

A-31710

NATIONAL AERONAUTICS AND SPACE ADMINISTRATION
AMES RESEARCH CENTER, MOFFETT FIELD, CALIFORNIA

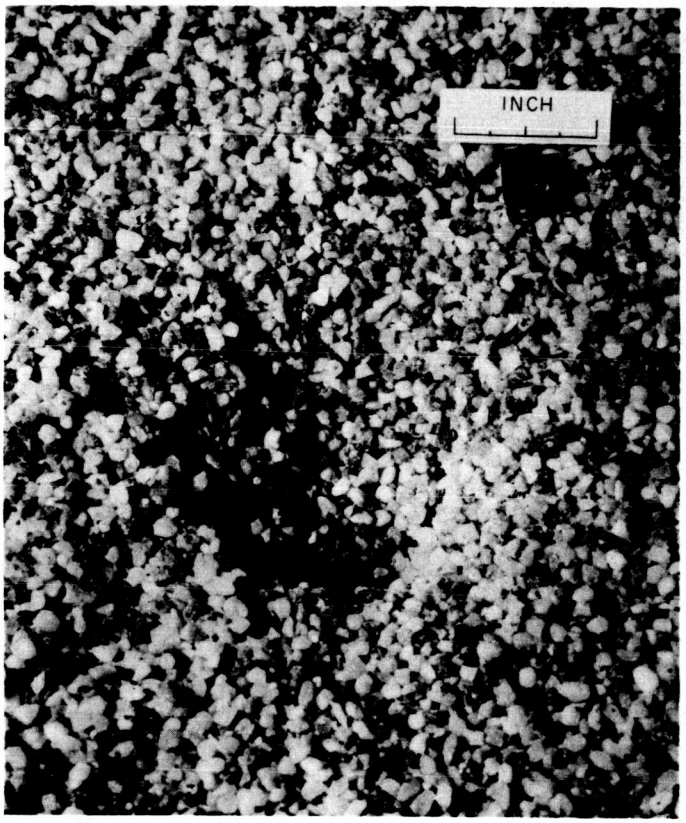

Figure 8.

A-30257

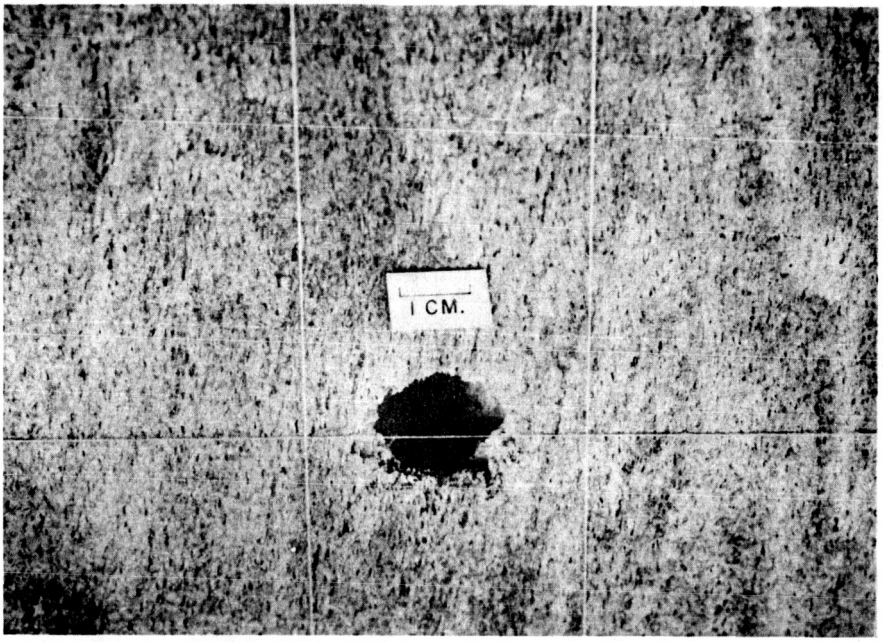

A-31578

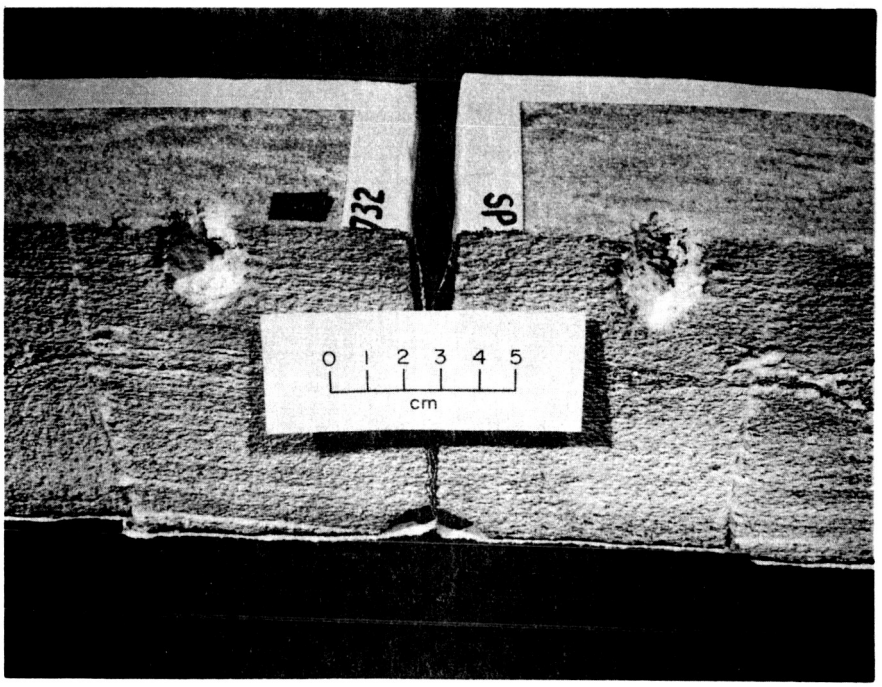

A-31588

Figure 9.

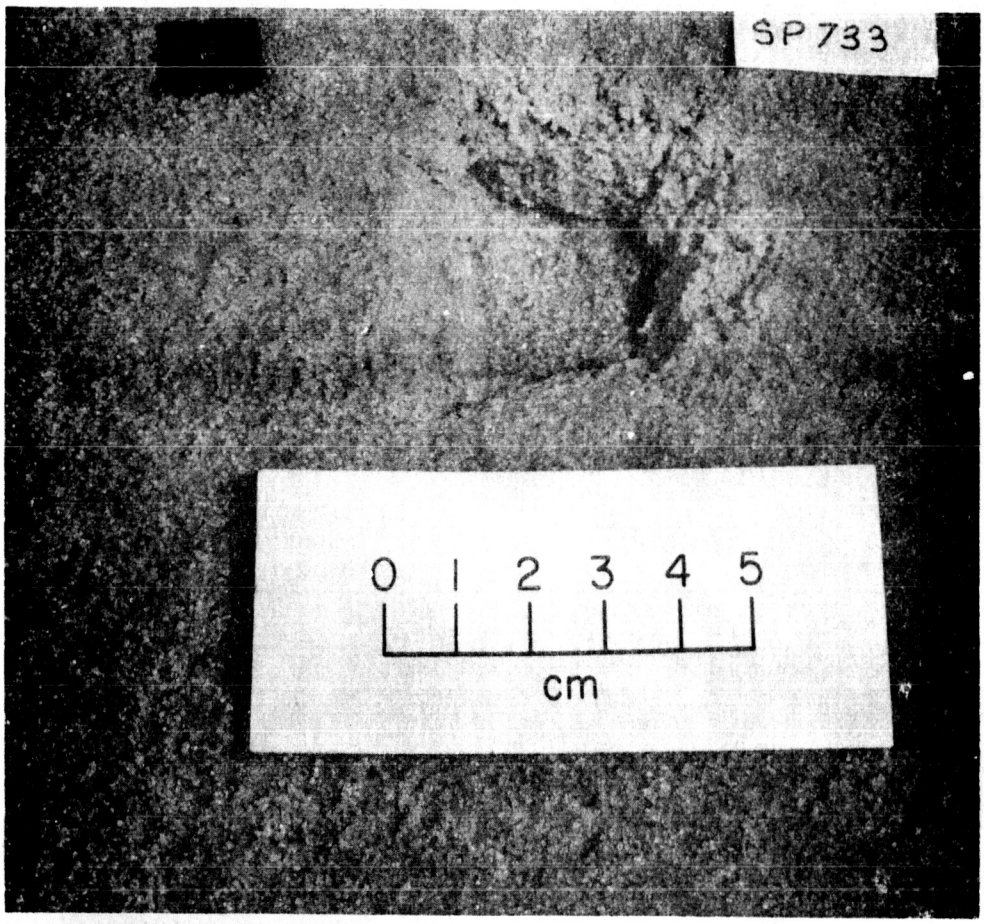

Figure 10.

A-31590

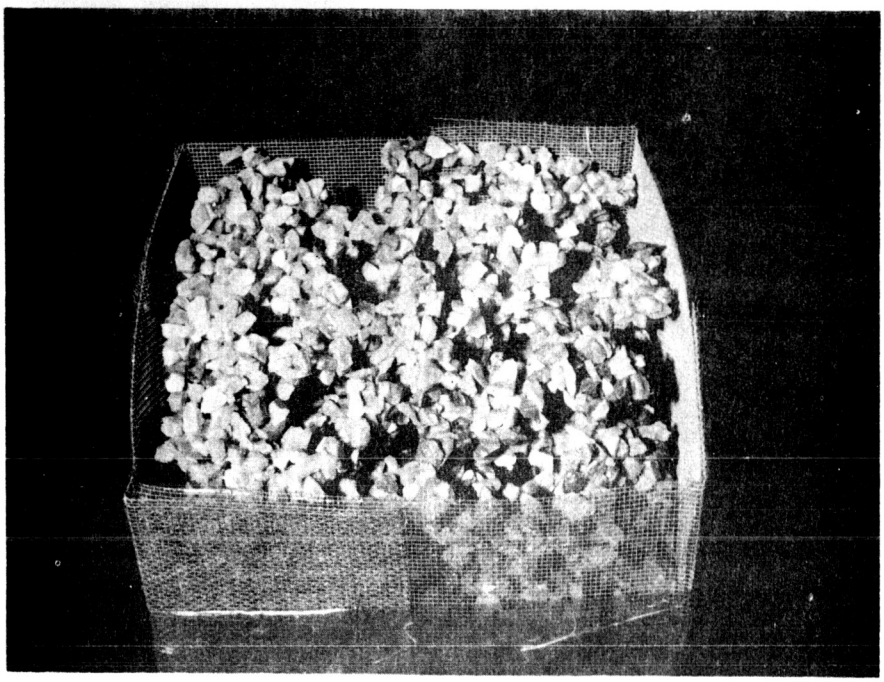

A-31335

Figure 11.

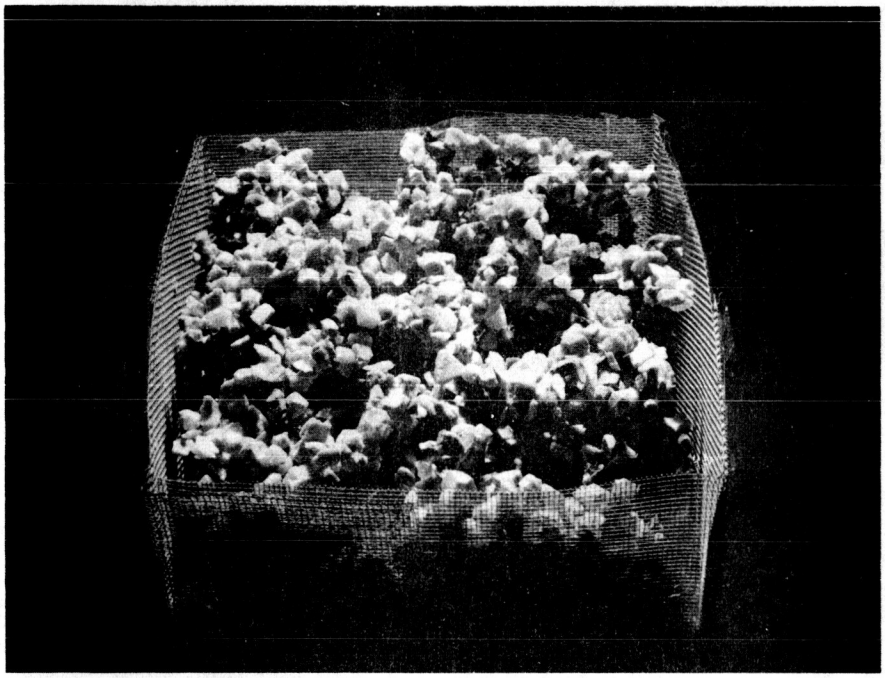

A-31337

Figure 12.

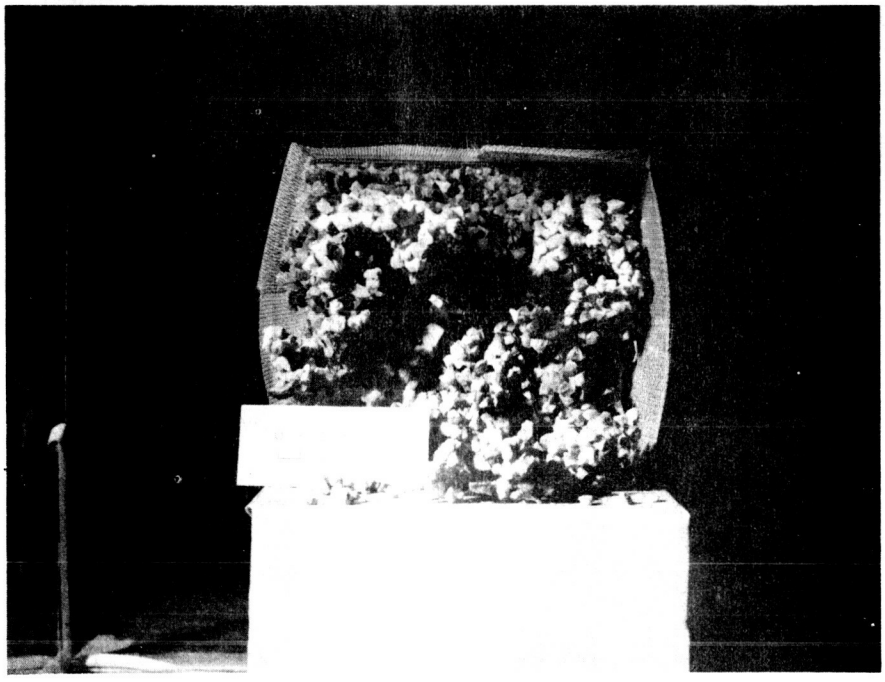

A-31585

Figure 13.

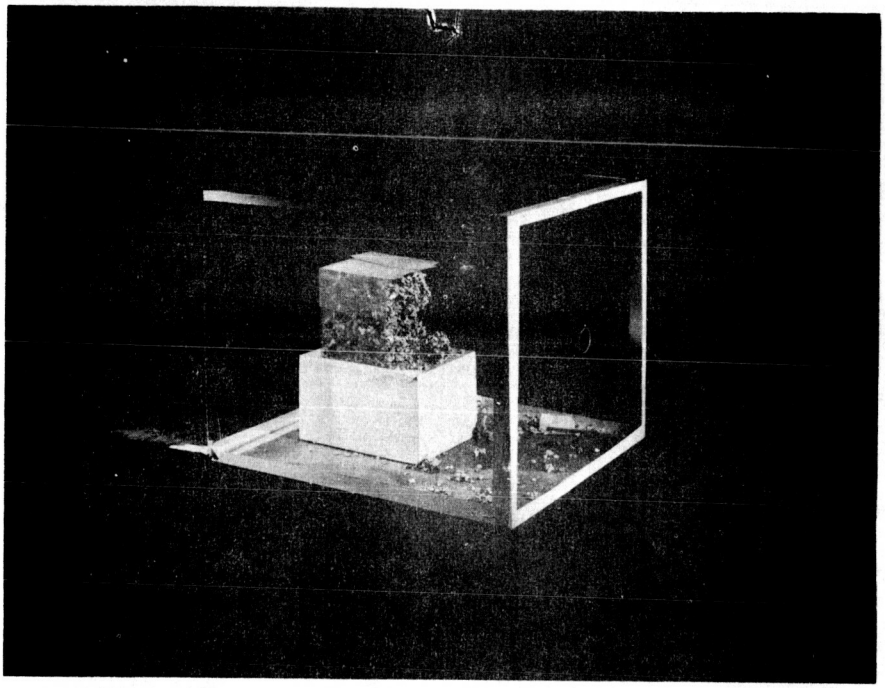

A-31587

Figure 14.

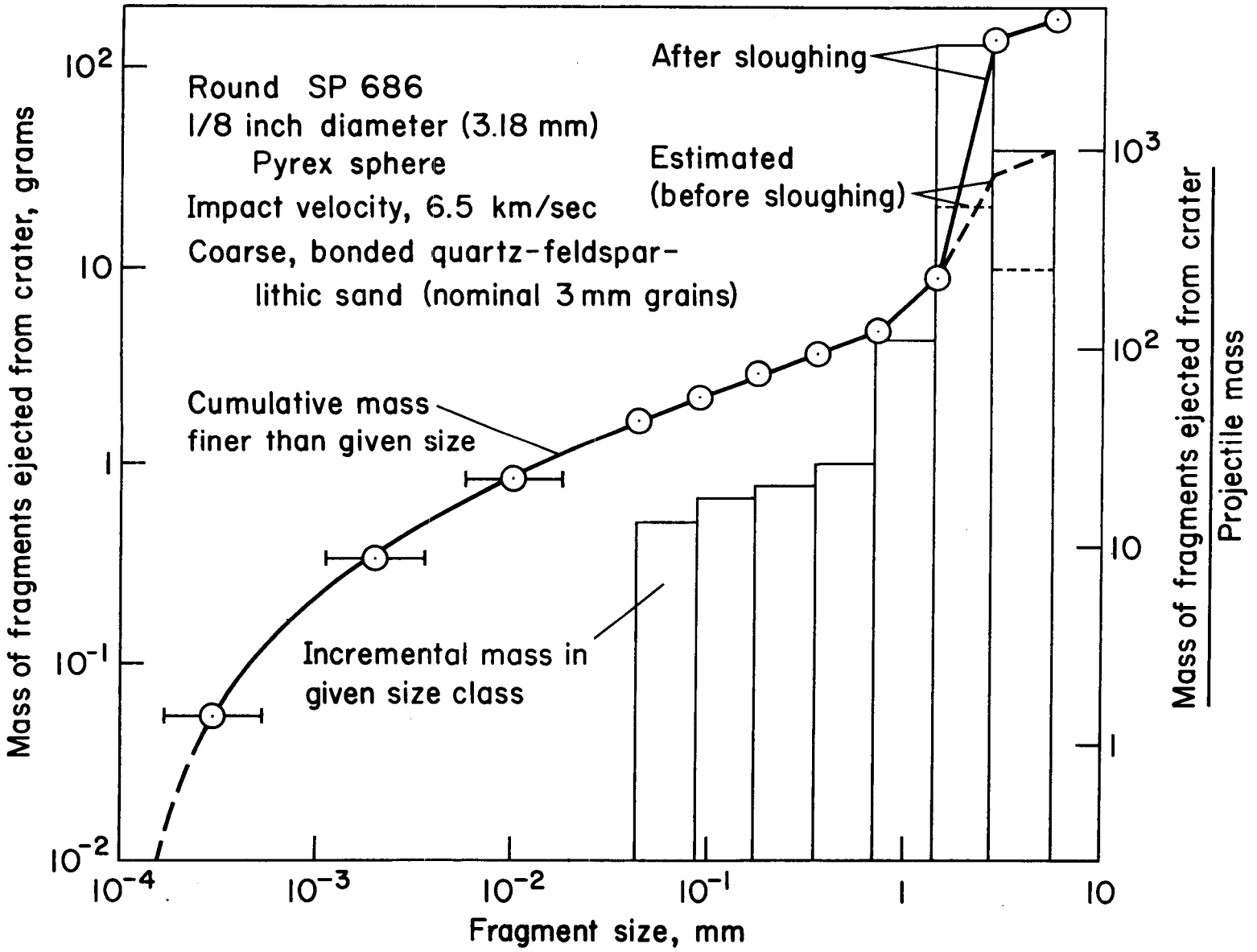

Figure 15.

NATIONAL AERONAUTICS AND SPACE ADMINISTRATION
AMES RESEARCH CENTER, MOFFETT FIELD, CALIFORNIA

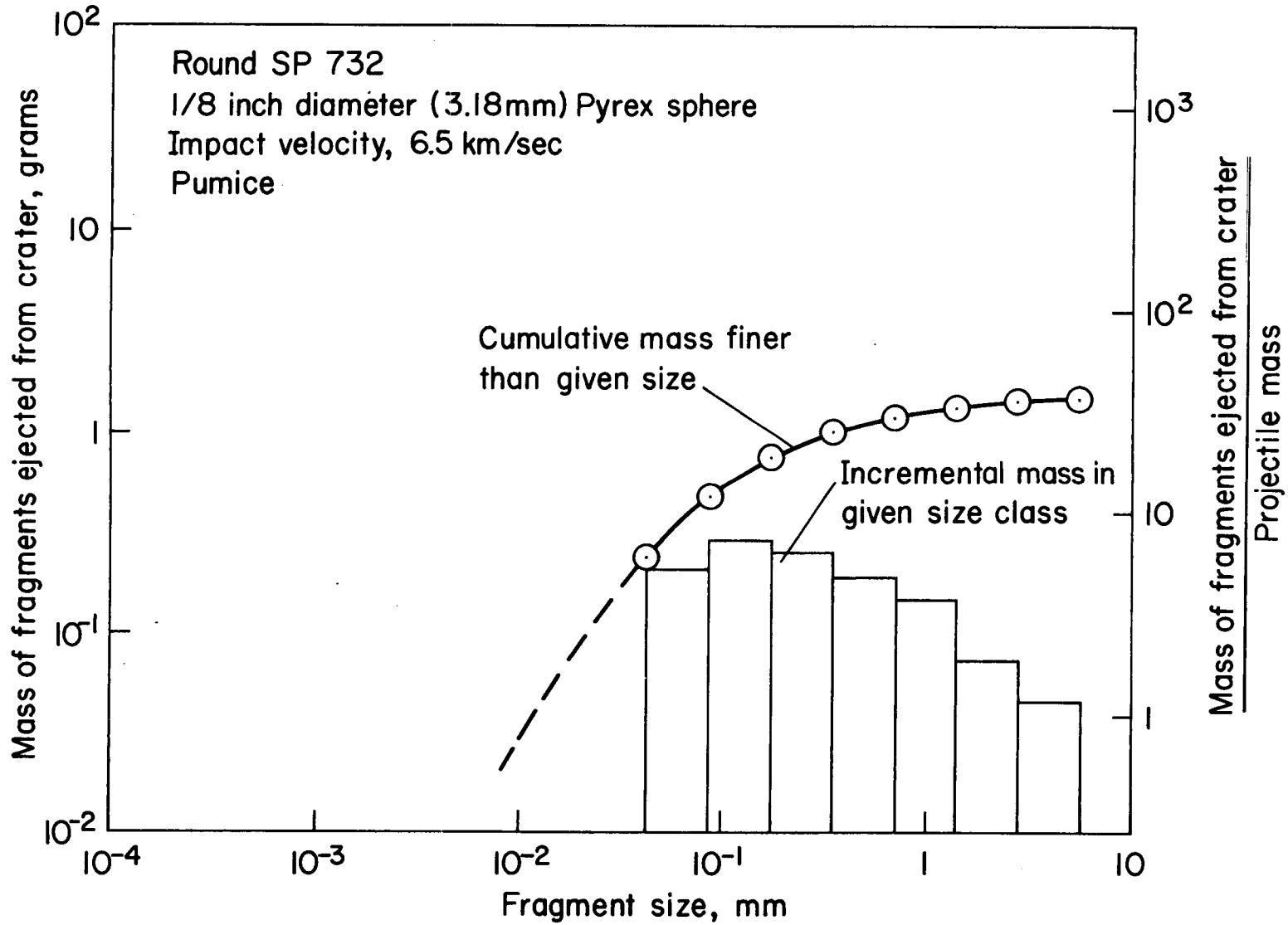

Figure 16.

NATIONAL AERONAUTICS AND SPACE ADMINISTRATION
AMES RESEARCH CENTER, MOFFETT FIELD, CALIFORNIA

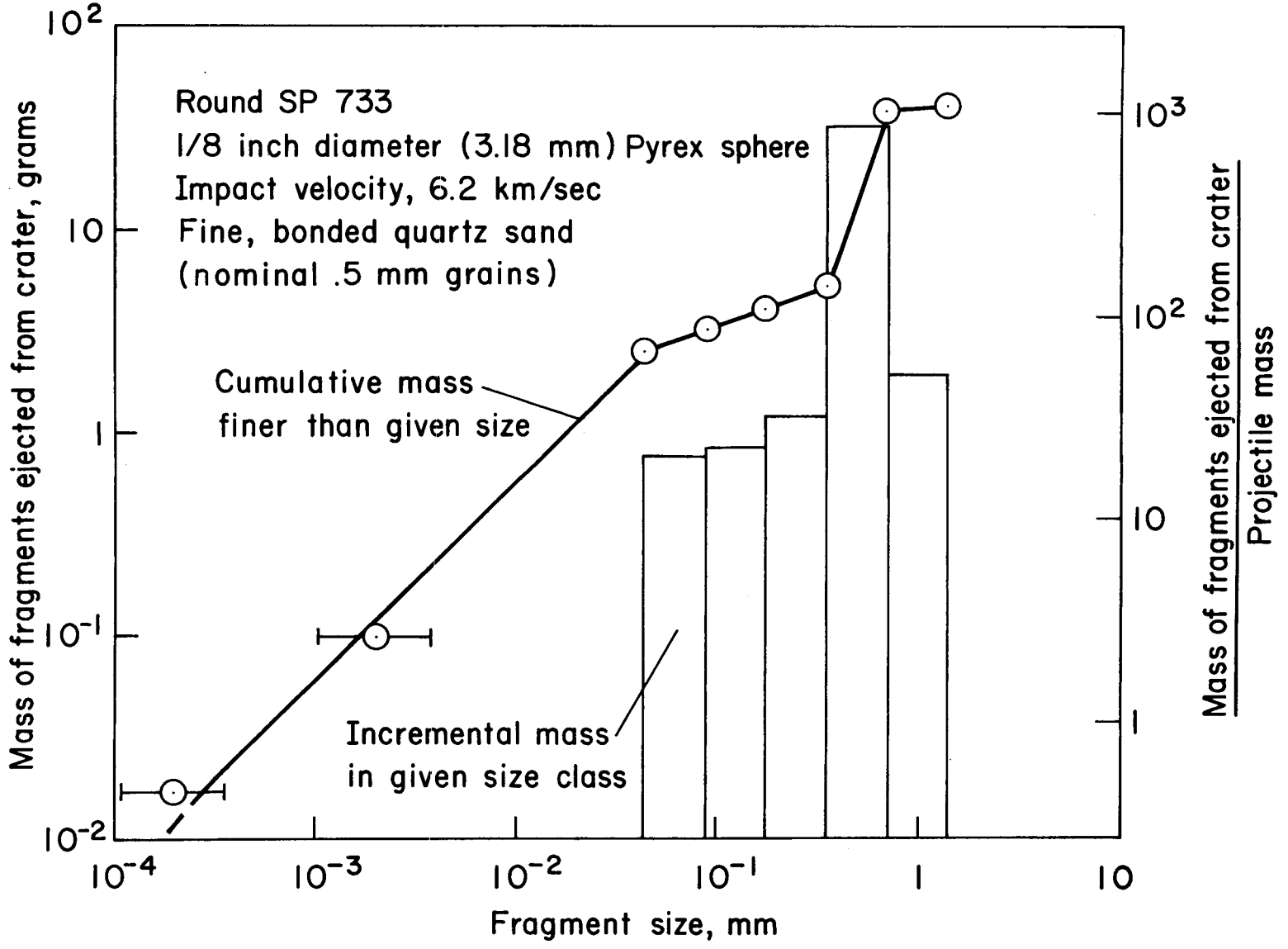

Figure 17.

NATIONAL AERONAUTICS AND SPACE ADMINISTRATION
AMES RESEARCH CENTER, MOFFETT FIELD, CALIFORNIA